Flow Ripple Reduction in Power Steering Hydraulic Pumps

Leonardo Zanetti Rocha*, Nigel Johnston and Samir N.Y. Gerges***

* Federal University of Santa Catarina (UFSC)
** University of Bath

ABSTRACT

Noise in hydraulic power steering systems is mainly generated by the hydraulic pump due to the cyclic pumping mechanism that creates pulsating flow transmitted by the fluid. This flow ripple and pressure ripple, propagating through the hydraulic circuit, interacts in a complex way with the other parts of the vehicle, generating audible noise inside the vehicle. The present work shows two ways to reduce the flow ripple amplitude generated by a vane pump through the redesigning of the pump rotating group. First, a nine-vane rotor pump is proposed and, secondly, a pump with three discharge ports is proposed. To check their results, a MatLab/Simulink based pump model was created according to the new geometrical characteristics and the results are compared with the regular pump ones. Also, a flow ripple experimental test was run using the Secondary Source Method to validate the numerical model results of the regular pump. The new designs simulation results show large flow ripple amplitude reduction (from 6dB to 16dB per harmonic) as well as frequency displacement in the discharge flow ripple spectra in both designs. Also, the simulations show perpendicular force on the pump shaft generated by the non-balanced conditions created by the new designs.

1. INTRODUCTION

Noise produced by the hydraulic power steering pump during the car operation can, in some situations, be perceived inside the vehicle as an annoying sound. The flow variations (flow ripple) generated by the pump through its natural operating process, are transmitted along the power steering hydraulic circuit, interacting with the impedance of the hoses and tubes generating structural vibration and sound emission around the circuit.

In some vehicles, the hydraulic circuit is tuned in order to avoid perceived noise inside the cabin. Flexible hoses, sometimes with tuning cables, are usually used to increase circuit compliance in order to remove unwanted frequencies or reduce the flow ripple amplitude. In fact, there are several techniques and devices (like silencers, side branches, accumulators, etc) that can be used to reduce fluidborne-noise along the propagation circuit [1, 2].

However, if a pump can be produced with a lower noise profile, this may create a solution that is independent of the hydraulic circuit and that does not require costly and time-consuming tuning of the system to achieve the wanted perceived noise reduction.

The present work is aimed at vane pumps and proposes two new rotating group designs, aimed at flow ripple amplitude reduction.

In order to achieve those results, a MatLab/Simulink based numerical-model is created from a regular pump design and validated through the experimental Secondary Source Method, developed in the University of Bath [3-5]. The simulated results of each new design are compared with the regular pump ones. Comparison is made in terms of the flow ripple amplitudes, and also in terms of force fluctuations.

2. PUMP MODEL

The numerical model of the pump is based on the general continuity equation, choosing the chamber (between a leading vane and its trailing vane) as the control volume. Similar models were created by Dickinson et al [6], Chalu [7] and Yang [8].

All the dimensions (geometric data) were loaded into the model from the drawings of a regular ten-vane automotive hydraulic pump. The pressure variation is described by equation 1:

$$\frac{dp}{dt} = -\frac{B_e}{V}\frac{dV}{dt} - Q_{IN} - Q_{OUT} - Q_{LEAK} \tag{1}$$

where Q_{IN} is the flow in the inlet port, Q_{OUT} the flow in the discharge port, B_e the effective bulk modulus, V the chamber volume and Q_{LEAK} the flow resulting by the leakage path inside the pump.

The flows through the inlet and outlet ports are calculated using the orifice equation, which relates the pressure difference between the downstream and upstream sides of a restriction:

$$Q = C_d A \sqrt{\frac{2\Delta p}{\rho}} \tag{2}$$

where C_d is the orifice flow coefficient, A the orifice area, ρ the fluid density and Δp the pressure difference between the upstream and downstream sides.

The flow leakages are calculated using the equation for laminar leakage flow between two planes, with one of them moving:

$$Q_{LEAK} = \frac{Lh^3(p - p_a)}{12\mu t} \pm \frac{uLh}{2} \tag{3}$$

where h is the clearance, L the width of the gap, t the length of the gap, ω the fluid viscosity and u the velocity. The first term of this equation describes the flow through the areas when both are fixed. The second term adds the effect of relative movement of the plates (Couette flow).

Analysing the pump operation and the way how the internal parts are assembled, several leakage paths can be identified where leakage flows can be calculated. So, equation 3 is used to calculate the following leakage paths into the pump rotating group.

Vane tip leakage:

$$Q_{vtl} = \frac{L_v h_1^{\,3}(p - p_a)}{12\mu t} \pm \frac{\omega r L_v h_1}{2} \tag{4}$$

Vane end leakage:

$$Q_{vll} = \frac{(r_c - r_r)h_2^3(p - p_a)}{12\mu t_v} \pm \frac{\omega(r_c + r_r)(r_c - r_r)h_2}{4} \tag{5}$$

Vane slot leakage:

$$Q_{vsl} = \frac{L_v h_3^3(p - p_{out})}{12\mu\left[h_v - (r_c - r_r)\right]} \tag{6}$$

where L_v is the vane length, h_1 vane tip clearance, h_2 the vane end clearance, h_3 vane slot clearance, ω the rotational speed of the vanes, p the fluid chamber pressure, p_a is the adjacent (leading or trailing) fluid chamber pressure, h_v the vane height, r_c the radius of the cam ring from the centre of the rotor, r_r the rotor radius.

Figure 1 shows a schematic of a fluid chamber showing the three leakage paths corresponding to equations (4), (5) and (6). The schematic also shows a leakage path across the end faces of the rotor, q_{rli}, which is not included in the current model as it is expected to be small.

The model also needs to include the 'under-vane' flow to the chambers at the inner radial faces of the vanes, caused by the vane movement:

$$Q_{uv_i} = v_i L_v t_v \tag{7}$$

where $v_i = -\,dr_i/dt$ is the radial speed of the vane. These chambers connect to the delivery port, and the pressure helps the vane with its radial movement to maintain contact against the ring wall, along with centrifugal forces. The sum of the under-vane flows results in the pump under-vane flow.

$$Q_{uv} = \sum_{i=1}^{N_v} Q_{uv_i} \tag{8}$$

where N_v is the number of pump vanes (in the standard pump, $N_v = 10$).

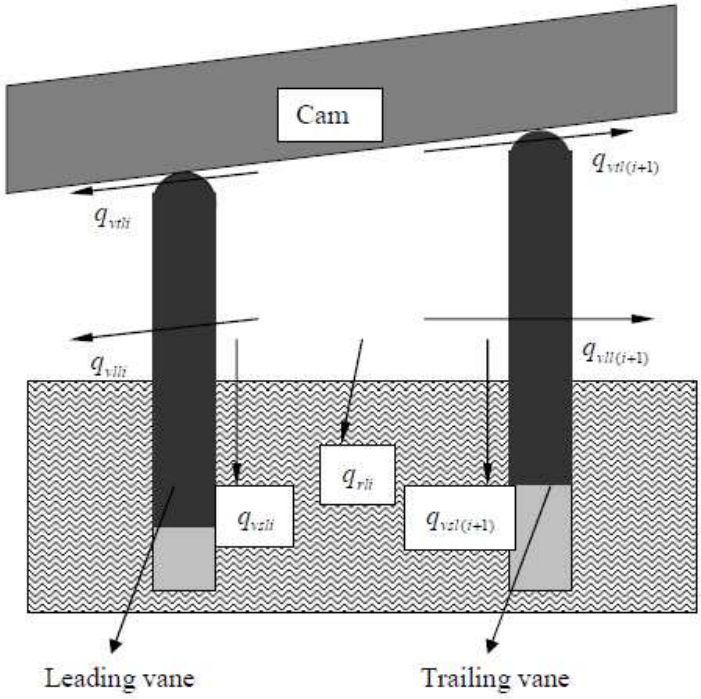

Figure 1 – Leakages flows into and out of the fluid chamber (from Chalu [7])

Some of the properties used in the simulation are listed in table 1. The fluid bulk modulus is reduced to allow for the effect of air bubbles and compliance of the rotor and vanes. The vane end clearance was estimated from the vane and rotor dimensions. The vane tip and vane slot clearances are simple estimates, and in practice these clearances would be expected to vary as the vanes move through their cycle.

Table 1 Properties used in simulation

Fluid viscosity	8.3 cP
Fluid density	870 kg/m^3
Effective bulk modulus	4×10^8 Pa
Flow coefficient for ports	0.6
Vane tip clearance	0.01 mm
Vane end clearance	0.019 mm
Vane slot clearance	0.01 mm
Rotor radius	20.7 mm
Rotor width	16 mm

3. SECONDARY SOURCE METHOD

The Secondary Source Method (SSM), developed at the University of Bath [3-5], was used to measure the pump flow ripple and the impedance.

The SSM is based on the measurements of the harmonics of pressure ripple at a series of points along the length of a rigid pipe connected either to the delivery and suction port of the test pump. The pressure ripple that occurs at two or three positions is analyzed to determine the pressure ripple.

From the Norton model shown in figure 2, is possible to find an equation to establish the pump flow at the discharge port:

$$Q_0 = Q_S - \frac{P_0}{Z_S} \tag{9}$$

where Q_s is the internal source flow, Q_0 the flow ripple at the pump discharge port, P_0 the pressure ripple at the discharge port and Z_s the source impedance.

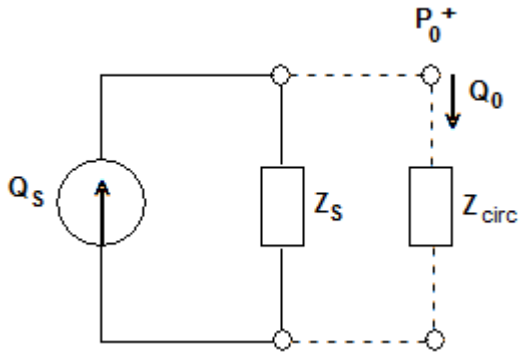

Figure 2 – Norton model of a pump.

In order to calculate the source impedance, a secondary source is situated downstream of the pump as shown in Figure 3. It can be shown that, if the second pump flow ripple frequencies do not coincide with the pump under test harmonic frequencies and the spectral leakages is negligible, Q_s can be assumed to be zero. So, equation 9 is simplified and the source impedance can be calculated as:

$$Z_S = -\frac{P_0}{Q_0} \tag{10}$$

Measurements of pressure ripple are then taken with the secondary source not operational, from which Q_s can be calculated easily through the Norton model given that Z_s, P_0 and Q_0 are known.

Even though the basic principles of SSM are presented, is not the aim of this paper to discuss it detail. More information and the detailed evaluation of the SSM can be found in [3] to [5].

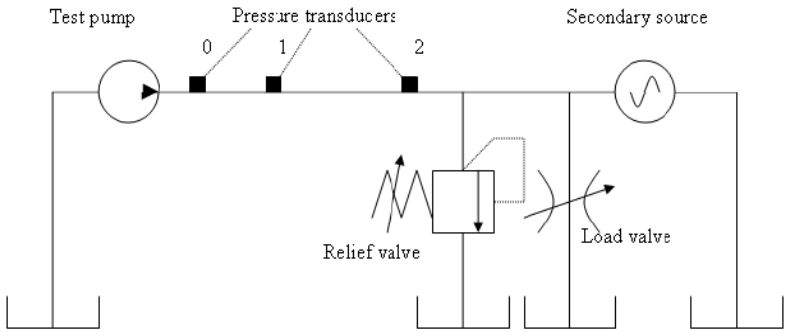

Figure 3 – Hydraulic Circuit for secondary source method [3].

The simulated results were compared with the experimental ones (measured using the SSM) and some results are shown in figure 4. These results show reasonably good agreement when the pump is run at low speed (1000 rpm in figure 4 (a) and (b)). However, for more extreme conditions (2000 rpm and 75 bar, figure 4 (c), for example), the shape of the flow does not match accurately with the simulated ones.

Whilst there are differences in the shapes of the waveforms, the peak-to-peak amplitudes are quite similar. Differences in the experimental and simulated results may be attributed to inaccuracies in the SSM as well as simplifications and assumptions in the simulation model. Uncertainties in the nature of the delivery passageway and integral flow control valve, which are not included in the model, may explain some of the differences. Nonetheless, the similarity in the amplitude and the trends of the results indicate that the results from the simulation model are reasonable and may be used to investigate the effect of changes in the design of the rotor, cam and ports.

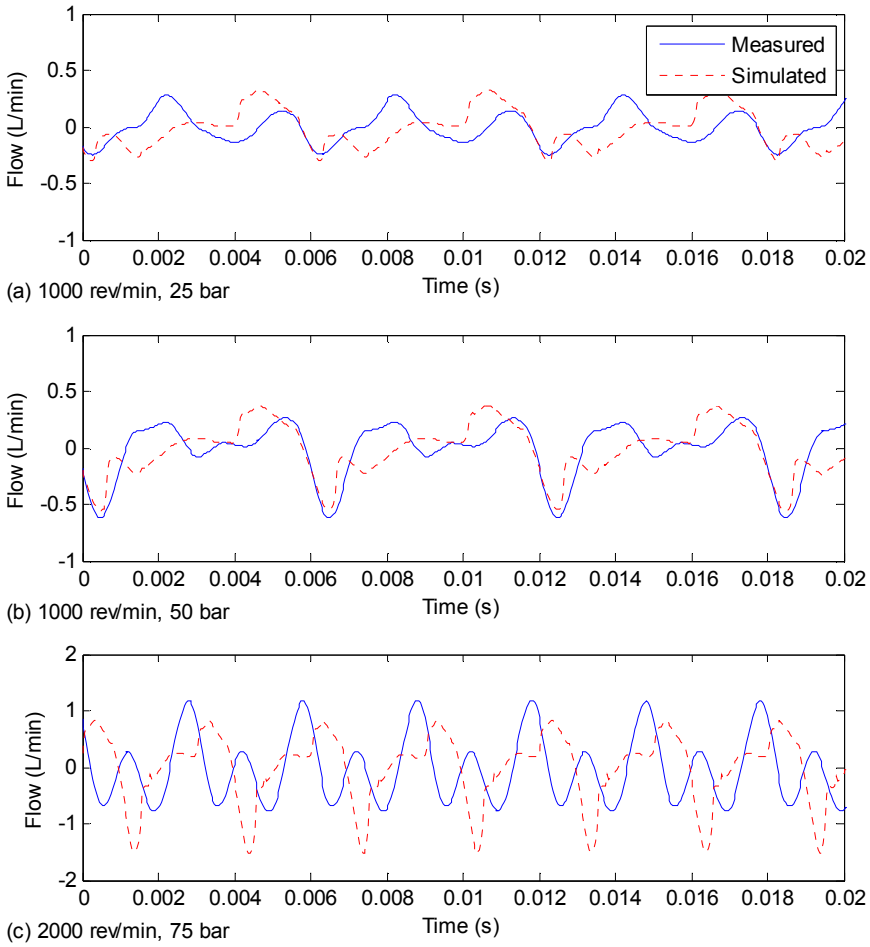

Figure 4 – Measured and simulated outlet flow ripple

4. NEW PUMP DESIGNS

4.1 Regular pump.

The regular automotive pump has two discharge ports located diametrically opposite each other, i.e., they are spaced by an angle of 180° regarding the centre of the thrust plate as the centre of the reference circumference. This kind of positive displacement pump is a so called *balanced pump* because these two opposite ports balance the force acting against the rotor (and all the walls of the chamber as well), reducing the shaft pump oscillations and overall vibrations. Figure 5 shows the inlet and outlet flow generated by just one fluid chamber. For this and all subsequent results the speed and pressure were 1000 rpm and 50 bar respectively, and all results were from simulation.

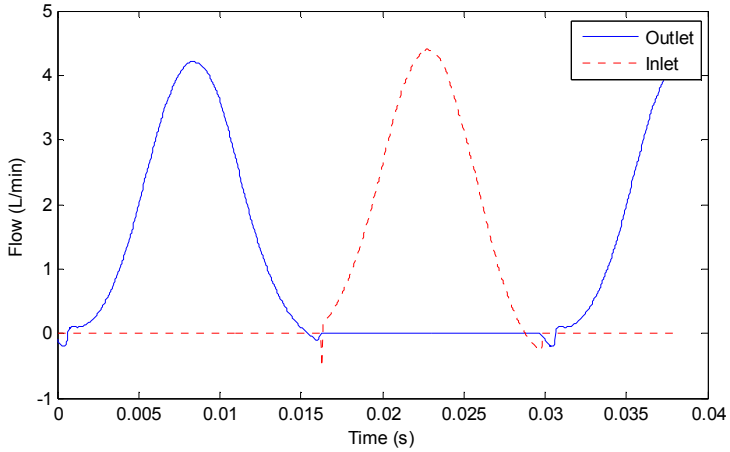

Figure 5 – Inlet and outlet flow for one fluid chamber.

As a result of this design, the discharge flow will be composed of the sum of the ten fluid chamber volumes per revolution.

The simulated waveform and amplitude spectrum of the flow at the discharge port are shown in Figure 6. The fundamental frequency f_0 is equal to the vane passing frequency f_V ($f_0 = f_V = \frac{N_V \Omega}{60} = 167$ Hz at 1000 rpm). This is the first and highest peak in the graph. Several smaller harmonics can also be seen.

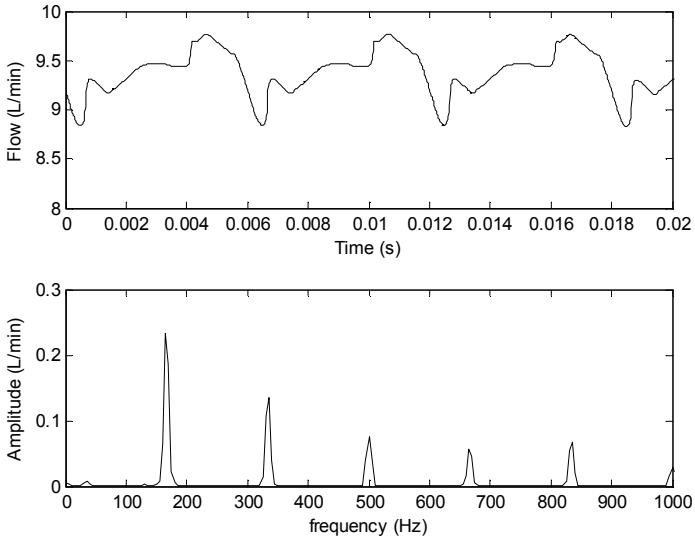

Figure 6 – Waveform and amplitude spectrum of total flow at outlet port.

4.2 Nine-vanes Pump.
In this design, the pump is modelled based on a rotating group containing a nine-slot rotor where the (nine) vanes are housed. The slots are equally spaced by an angle of 40° to each other while the other parts (ring and plates) remain the same. Figure 7 shows the rotor cross-section.

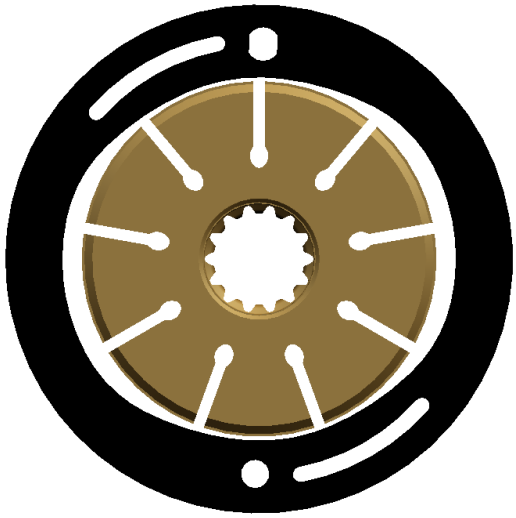

Figure 7 – Nine-vane rotor and cam.

Unlike what is found in the regular pump, where the diametrically opposite vanes (for example, the first and sixth vane) reach the discharge ports at the same time, in this nine-vanes design the opposite vanes will reach the respective discharge port in a different time, offset by a rotational angle of (40/2)°. The effect of this process is the destructive interference of the chambers' discharge flows at the outlet port, generating an increase in the flow ripple frequency and reduction in the amplitude. The predicted flow ripple waveform and amplitude spectrum are shown in Figure 8.

The mean flow level remains roughly the same in both regular and 9-vane pumps. This is because the cam profile is the same in both cases. The displacement in frequency and the amplitude reduction are clearly shown in Figure 8. Because the ports open alternately, the fundamental frequency f_0 is now given by $f_0 = 2f_V = \frac{2N_V\Omega}{60} = 300$ Hz. There is a great improvement moving the fundamental to higher frequency because the noise isolation of the hydraulic circuit tends to be better at high frequencies, further helping to reduce the noise. However the human ear is more sensitive to these higher frequencies. The tonal characteristic will be quite different, and the perception by the occupants of the car would need to be considered subjectively [9, 10].

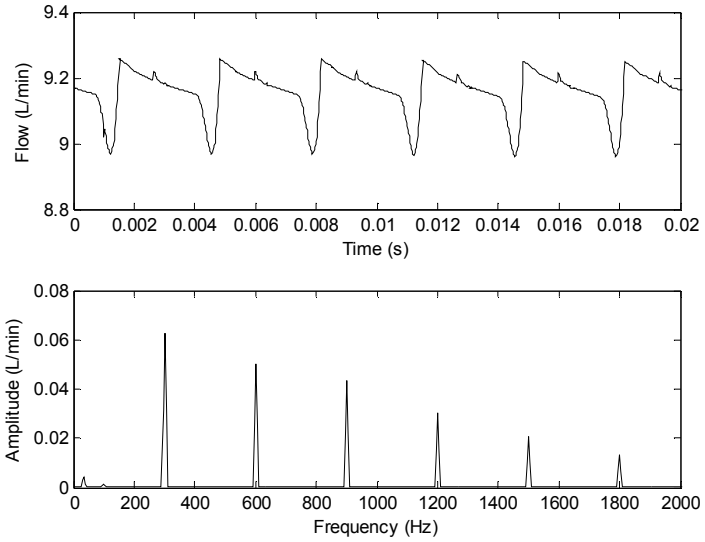

Figure 8 – Total flow at outlet port of the nine-vane design.

4.3 Three discharge port Pump.

In this design, the pump is modelled based on a rotating group composed of a standard ten-vane rotor but with three discharge and suction ports in the thrust and pressure plates. Also, the cam ring is redesigned to support the new plate's modifications as shown in Figure 9.

The 3 suction ports are spaced by an angle of 120° between themselves as well as the discharge ports. Each discharge and suction port has a radial length of 24° while the "pre-compression" zone (situated between the suction and discharge port) has a radial length of 36°, keeping the minimum angle between a leader and a trailing vane to avoid "short-circuit" between the ports. The cam profile was designed to give the same displacement as the other designs.

With this configuration, a fluid chamber reaches the beginning of a discharge port every 12° of rotation. For example, when a vane reaches the very beginning of the first discharge port, another vane will be in the middle of the second discharge port and another vane will be in the end of the third discharge port. This happens the same way in the suction port. The result of this three-phase fluid delivery is, again, the destructive interference of each delivered fluid *package*, achieving excellent outlet flow amplitude reduction. Figure 10 shows the flow ripple waveform and amplitude spectrum. The steady flow level is roughly the same as for the regular pump.

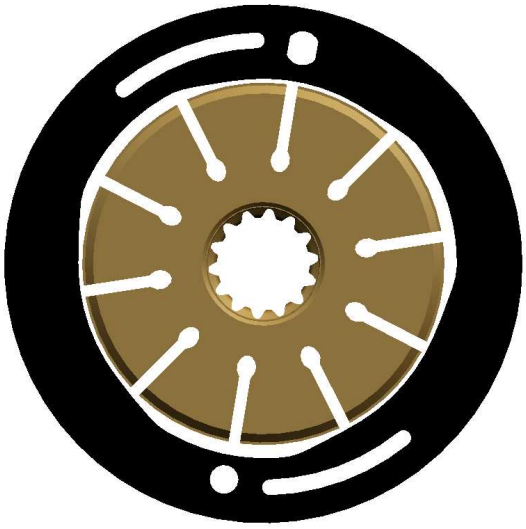

Figure 9 – Three-port cam ring internal profile.

As with the nine vanes design, in this three-port design there will be displacement in the frequency-domain. Now, the fundamental frequency f_0 changes from 167 Hz (regular pump) to $f_0 = 3f_V = 500$ Hz, changing the original tonal pump noise.

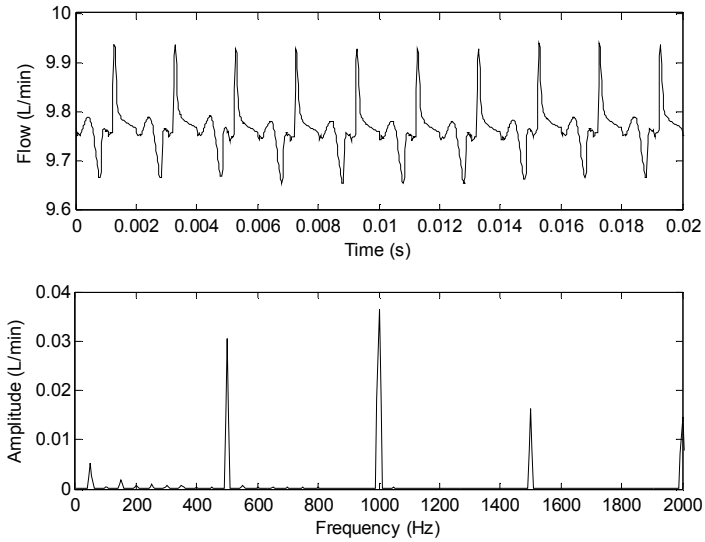

Figure 10 - Total flow at outlet port of the three discharge port design.

Figure 11 shows the reduction achieved per harmonic for each new design. This result shows a reduction around 12dB (9 vanes design) and 16dB (3 ports design) regarding the

first harmonic of the generated noise, and similar reductions for the higher harmonics. From the graph, it's possible to conclude that the 3 ports design gives the best flow ripple reduction. It should be noted that the timing of the ports and relief grooves, and the shape of the cam ring, may not be ideal for the new designs, and further improvement could be achieved by optimising the design.

Also, the frequency displacement will help the vehicle system to absorb the noise, as the high frequencies may be easier to reduce through the transmission path (fluid and air) than the low ones, and there are likely to be fewer significant harmonics.

Unfortunately the proposed designs result in instantaneous force imbalances because of the alternating port opening. The undesirable effect of these two new designs is shown in Figures 12 and 13. These graphs show the resulting perpendicular forces on the shaft and rotor during the pump operation. These were computed from the simulated pressures acting on the rotor and vanes. In the regular pump the theoretical forces would always be zero. For the modified designs there is a rapid and large force fluctuation.

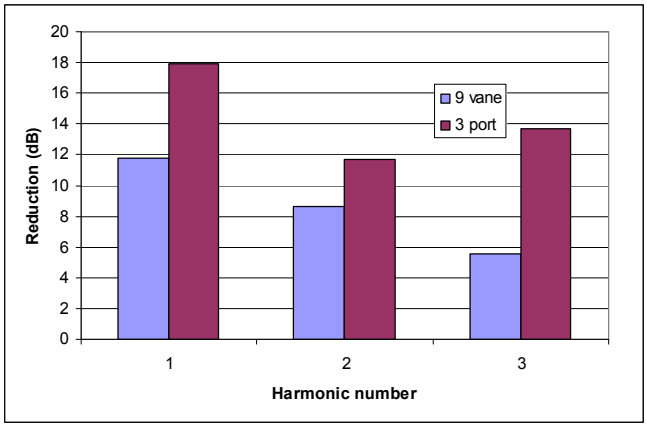

Figure 11 – Reduction in amplitude versus harmonic for the nine-vane and three-port pump designs, relative to the regular design.

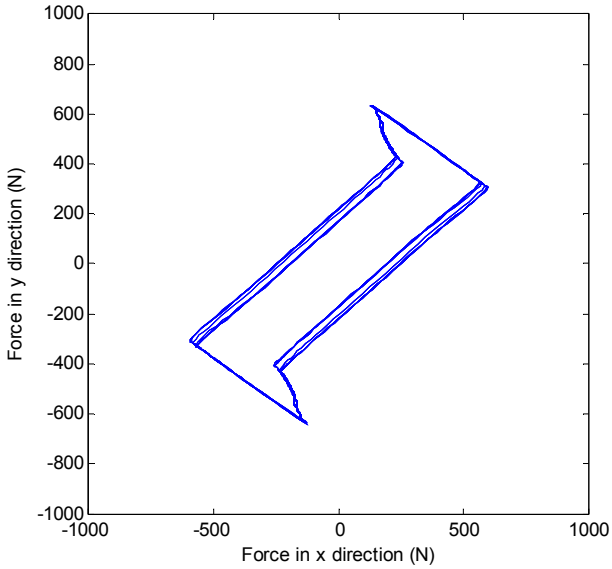

Figure 12 – Resulting lateral forces on rotor, nine-vane design.

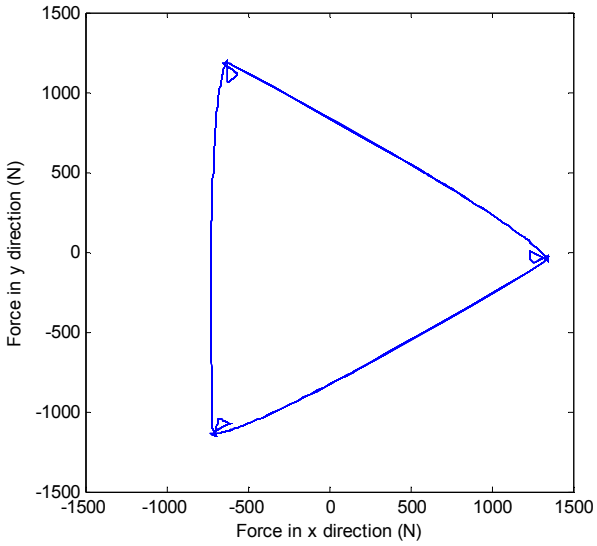

Figure 13– Resulting lateral forces on rotor, three-port design.

These resulting forces may generate excessive vibration on the shaft or housing, causing wear or even mechanical damage to the shaft bearing. Therefore, the practical use of these new rotating group designs in the regular automotive pump needs strategies to reinforce the shaft-bearing to avoid undesirable vibration and damage.

5. CONCLUSIONS

This work has shown a method to calculate and predict the outlet flow in an automotive positive displacement pump. Also, it presented an experimental method (Secondary Source Method) to rate the pump flow ripple that was used to validate the numerical results.

Two new rotating group designs were proposed; a nine-vane and a 3 port design, aiming for flow ripple amplitude reduction and frequency increase. Both designs have shown excellent flow ripple amplitude reduction (over 10dB for the first harmonic in both designs) and a displacement of the tonal noise frequency. Both effects, allied with the vehicle noise isolation capability, can improve the noise acoustical comfort and reduce the perceived noise inside the vehicle.

Nevertheless, these new designs showed an undesirable effect, presented by the non-compensated forces over the shaft-end. These resulting forces could generate extra shaft vibration and wear if the shaft and bearings are not properly designed to support those unbalanced forces.

REFERENCES

1 Gerges, S., Johnston, D.N., Rocha, L. Z. *Noise and Vibration in Fluid Power Systems*. Handbook of Hydraulic Fluid Technology, Taylor & Francis group, Florida, US, 2010.

2 Skaistis, S., *Noise control of hydraulic machinery*, Marcel Dekker, New York

3 Johnston, D.N. *Measurement and Prediction of the Fluid Borne Noise Characteristics of Hydraulic Components and Systems*. PhD Thesis, University of Bath, UK, 1987.

4 Edge, K.A., Johnston, D.N. *The `secondary source' method for the measurement of pump pressure ripple characteristics, part 1: description of method*, Proc IMechE, part A, vol. 204, 1990, pp33-40

5 Edge, K.A., Johnston, D.N. *The `secondary source' method for the measurement of pump pressure ripple characteristics, part 2: experimental results,* Proc IMechE, Part A, vol. 204, 1990, pp41-46

6 Dickinson A L, Edge K A, Johnston D N, *Measurement and prediction of power steering vane pump fluidborne noise*, SAE Transactions - Journal of Passenger Cars, vol 102, sect 6, 1993, #931294, pp1753-1761

7 Chalu, C. *Torque fluctuations and vibrations in a vane pump*. MPhil Thesis, University of Bath, UK, 2004

8 Yang, M. *Modelling and Analysis of pressure pulsations in hydraulic components and systems with particular reference to pump fault diagnosis*. PhD Thesis, University of Bath, UK, 2009

9 Rocha, L.Z., Paul, S., Jordan, R., Gerges, S. *Sound Quality Evaluations of Hydraulic Pumps*. SAE paper 2008-36-0583, São Paulo, 2008.

10 Leite, R.P., Paul., S. *Sound Quality: Basic concepts illustrated with an automotive field example.* Brazilian Acoustical Society magazine (SOBRAC), nº 37, Brazil, 2006.